Ad Hoc Networks 135 (2022) 102946

Contents lists available at ScienceDirect

Ad Hoc Networks

journal homepage: www.elsevier.com/locate/adhoc

Multi-class random access wireless network: General results and performance analysis of LoRaWAN

F. Helder C. Santos F. [a], Plínio S. Dester [b,1], Pedro H.J. Nardelli [c,d,*,2,3], Elvis M.G. Stancanelli [a], P. Cardieri [b,1], Dick Carrillo [c,4,3], Hirley Alves [d,2,5]

[a] Federal University of Ceará, Quixadá Campus, Quixadá, 63902-580, Brazil
[b] School of Electrical and Computer Engineering, University of Campinas, Brazil
[c] LUT University, Finland
[d] University of Oulu, Finland

ARTICLE INFO

Keywords:
LoRa
Spreading factor allocation
Multi-class wireless network

ABSTRACT

This paper presents new analytical results for evaluating the ALOHA-like multi-class random access wireless network's performance. The proposed model is motivated by the growth of low-power wireless networks that employ random access protocols. In particular, we compare our analytical formulation with system-level simulations of Long Range (LoRa) technology. We show that the proposed formulation provides an accurate approximation of LoRaWAN performance capturing its main trade-offs. The main contributions are (i) an extensive analysis of the impact of different LoRa spreading factors (SFs) allocation strategies, including area intersection among SFs, which is little explored in the literature and represents the optimal approach under some conditions; and (ii) the optimal proportion of users that maximizes the network throughput for each class and for each allocation strategy considered in the paper.

1. Introduction

The interest in multi-class random access wireless networks is rising due to the significant growth of internet of things (IoT) applications. The spotlight turns to the machine type communication (MTC) technologies, where many devices can communicate with each other and with servers in the cloud, constituting a cyber–physical system. In this context, one of the critical aspects of 5G systems is MTC communication, divided into two major areas, namely massive communications (mMTC) and communications that require high reliability and low delay (uMTC) [1]. In particular, mMTC communication is related to applications with tolerance to delay, usually with a low transmission frequency, and a massive number of devices mainly operating on batteries.

Typical examples of mMTC networks are low-power wide-area (LPWA) technologies, which complement traditional cellular and short-range wireless technologies to meet the diverse requirements of IoT applications [2]. LPWA technologies offer a set of features not provided by legacy wireless technologies, including wide-area connectivity for a large number of devices, low energy consumption, and low data rate devices. Most LPWA networks operate on unlicensed industrial, scientific and medical networks (ISM) band. Some of the best-known candidates for LPWA networks are long range (LoRa), SigFox, NB-IoT, and LTE-M.

In this paper, we focus on LoRa technology, one of the most promising LPWA approaches, proposed by Semtech and further promoted by the LoRa Alliance [3]. LoRa is based on a variant of spread spectrum modulation (SSM) called chirp spread spectrum (CSS), which is robust under multiple path fading. CSS uses quasi-orthogonal SFs, in which the spectrum spreading is achieved by generating a chirp signal that varies continuously in frequency. Given this characteristic, LoRa resembles traditional ALOHA-like random access systems, but with different user classes of users related to the different SFs (ranging from 7 to 12) [4].

* Corresponding author.
E-mail address: pedro.nardelli@lut.fi (P.H.J. Nardelli).

[1] This paper is partly supported by Foundation for Research Support of the State of São Paulo, Brazil (Grant No. 2017/21347-0). This work as also financed in part by the Coordenação de Aperfeiçoamento de Pessoal de Nível Superior - Brasil (CAPES) - Finance Code 001.

[2] Senior Member, IEEE.

[3] This paper is partly supported by Academy of Finland via: (a) ee-IoT n.319009, (b) FIREMAN consortium CHIST-ERA-17-BDSI-003/n.326270, and (c) EnergyNet Fellowship n.321265/n.328869.

[4] Member, IEEE.

[5] This paper is partly supported by 6G Flagship (Grant n.318927), and ee-IoT (n.319008) and FIREMAN consortium (CHIST-ERA-17-BDSI-003/n.24303093).

https://doi.org/10.1016/j.adhoc.2022.102946
Received 13 January 2022; Received in revised form 17 June 2022; Accepted 11 July 2022
Available online 14 July 2022

With the number of devices increasing every day and an essential part of them connected via LPWA, understanding such networks' scalability is essential before their deployment. A strategy for allocating SFs for the nodes influences the network's overall performance. Thus, significant attention must be paid to the different SF allocation strategies. To extract the best from the different SFs for each scenario is necessary to establish the optimum allocation strategy.

The paper [5] is one of the first works that provides a theoretical analysis considering the co-SF interference. The mathematical formulation gives the achievable LoRa throughput in the uplink considering the standard scenario of no area intersection among SFs. The study in [6] modeled the LoRa network as several nodes operating at different frequencies and SF allocations. That paper addressed the challenges upon intra-SF and inter-SF collisions, using a numerical approach. The study consisted of many packet rates for each SF and several bandwidth configurations. The authors used numerical analysis to determine the percentage of nodes for each SF; it was done using configurations close to optimum compared to having the same number of nodes per SF. The results based on different bandwidth values, frequencies, and packet rates show that to achieve the nodes' capacity optimum, the percentage of nodes for each SF must be 77% and 23% for SFs 7 and 8, respectively, and 0% for the other SFs (9–12).

In [7], a system model for uplink communication in single gateway implementation is shown using stochastic geometry modeling. Two conditions are considered for the probability of interruption of a desired power signal on the uplink: if the power is above a specific signal-to-noise ratio (SNR) limit, and if the power is at least 6 dB stronger than the dominant co-SF interference. The work in [8] investigated the scalability of a LoRa network. The authors evaluated the interference due to the scalability resulting from imperfect orthogonality, focusing on a multi-annuli single-cell system, and based on the probability of coverage of the uplink under the combined effect of co-SF and interference. Along the same line, in [9], the authors propose a stochastic geometry model to evaluate the impact of co-SF interference and external interference from coexisting technologies. However, differently from [8], a reliability target is imposed for each SF, which leads to an optimal network configuration concerning coverage or minimum reliability.

The impact of SF distribution between nodes on the probability of success of the packet (PSP) is studied in [10], where the SF distribution regions are determined to increase the average PSP of the network. They adopt three existing schemes, i.e., equal-interval-based (EIB) (Equal Interval Based) scheme, equal-area-based (EAB) (Equal Area Based) scheme, and Random scheme, which allocates SFs by uniform random choice. When assigning SFs to the end nodes, two conditions are considered. The first condition is that the energy received from each node at the gateway must exceed the receiver's sensitivity limit for the assigned SF. The second condition is that the signal-to-interference ratio (SIR) must also exceed the correctly decoded SIR limit for that SF. An SF assignment optimization problem is formulated, where the average PSP of the network is maximized given the regions covered by each SF.

In [11], the authors tackle the scalability of a single gateway LoRa network. They propose a mathematical model based on stochastic geometry (nodes' positions follow a Poisson point process) that considers co-SF and inter-SF interference. They compare two SF allocation schemes: the standard EIB (Equal Interval Based) and the new proposed Success Probabilities and device Density (SPD), which allocates SFs based upon device spatial density and success probability. Note that both schemes do not consider area intersection among SFs. The authors show, through simulations, that the proposed SPD scheme improves 13% in respect to the EIB method in terms of success probability.

This paper derived a mathematical model applied to LoRa that considers multiple user classes and imperfect orthogonality. This model enables the investigation of SF allocation strategies in LoRa beyond the classical approach that considers concentric rings without intersection, including schemes such as EAB, EIB, and optimal cases, such as in [6–10]. This paper also advances the study and understanding of the SF effects, proposing new SF allocation techniques, which consider partial and total intersections of SFs. In our study, the nodes are grouped into user classes,[6] and each class uses an SF. We numerically optimized the SF allocation to find the region covered by each SF and its respective proportion of nodes in order to maximize the system throughput. We have considered different SF approaches as, for example, No Intersection (NI) for the classical approach; Full Intersection (FI) and Partial Intersection (PI) for new techniques.

Table 1
Notations and symbols used in the paper.

Symbol	Definition/explanation
$\mathbb{Z}, \mathbb{Z}_+$	Set of integers and non-negative integers
$\mathbb{R}, \mathbb{R}_+$	Set of real numbers and non-negative reals
$\mathbb{C}$	Set of complex numbers
$\mathbb{E}[\cdot]$	Expected value operator
i	Imaginary unit ($\sqrt{-1}$)
φ_X	Characteristic function of random variable X
G_N	Generating function of random variable N
n_c	Number of user classes
$\mathcal{N}$	$= \{1, 2, \ldots, n_c\}$ is the set of user classes
α	Path-loss exponent
δ	$\triangleq 2/\alpha$
a_i	Rate of packets per user class (ith class)
λ_i	Rate of packets per channel (ith class)
τ_i	Time on air (ToA) (ith class)
θ_{ij}	SIR threshold for successful communication (i receiving interference from j)
R_i	Transmission distance (ith class)

The paper is organized as follows: Section 2 presents and proves a general result on the distribution of interference with general fading and general path-loss function from a set of randomly distributed interferers. Then it presents the system model studied in the paper, for which we set an uplink transmission scenario from several nodes to a central gateway, then we prove two propositions on the transmission success probability; Section 3 introduces the parameters of a LoRa system used in the analytical model; Section 4 applies the analytical results in the uplink transmission of a LoRa system for several scenarios, and we compare the results between the theoretical model and Monte Carlo simulation, which is done using the discrete-event network simulator ns-3; Section 5 concludes the paper. The notations used in the paper are summarized in Table 1.

2. System model and analytical results

This section presents the system model along with some analytical results. We start with a general model of ALOHA-like multi-class random access network motivated by the LoRa setting to be discussed later and specialize it throughout the section because we require more constraints to obtain the analytical results.

2.1. Distribution of the interference

This subsection aims to derive the characteristic function of the interfering signal measured at a given point in a coverage area. The studied scenario constitutes of a random number of interferers transmitting at random distances. Here, the signal transmitted by each interferer is attenuated by fast fading and path-loss phenomena.

Let the path-loss function $\ell : \mathbb{R}_+ \longrightarrow \mathbb{R}_+$ be a monotonous decreasing function such that $\ell(r) \to 0$ as $r \to \infty$, the attenuation coefficient of the kth interferer be the random variable Z_k (which may include stochastic phenomena such as time of superposition or small scale

[6] Note that, in this paper, we named **user class** to refer to the users in the same SF that are of the same type device class A.

fading), the distance of the kth interferer to the point of analysis be the random variable R_k and let the number of interferers be represented by the random variable N. Then, the normalized interference power received at the point of analysis is given by

$$I = \sum_{k=1}^{N} Z_k \, \ell(R_k). \tag{1}$$

We aim at finding the distribution of the interference $F_I(\cdot) \triangleq \mathbb{P}(I \leq \cdot)$ as a function of the distribution of other random variables. For that, we need the following definitions. The characteristic function of a random variable X is defined as $\varphi_X(\omega) \triangleq \mathbb{E}[\mathrm{e}^{\mathrm{i}\omega X}]$, $\omega \in \mathbb{R}$ and the generating function of the discrete random variable N is defined as $G_N(z) \triangleq \mathbb{E}[z^N]$, $z \in \mathbb{C}$. Then, we can write the characteristic function of the interference in a compact notation, as follows

$$\begin{aligned}\varphi_I(\omega) &= \mathbb{E}\left[\exp\left(i\omega \sum_{k=1}^{N} Z_k \, \ell(R_k)\right)\right] \\ &= \sum_{n\in\mathbb{Z}_+} \mathbb{E}\left[\exp\left(i\omega \sum_{k=1}^{n} Z_k \, \ell(R_k)\right)\right] \mathbb{P}(N=n) \\ &= \sum_{n\in\mathbb{Z}_+} \left[\varphi_{Z\ell(R)}(\omega)\right]^n \mathbb{P}(N=n) \\ &= G_N\left(\varphi_{Z\ell(R)}(\omega)\right), \quad \omega \in \mathbb{R},\end{aligned} \tag{2}$$

where we use independence among the random variables.

Furthermore, the distribution of I can be calculated using the Gil-Pelaez inversion theorem [12]

$$F_I(x) = \frac{1}{2} - \frac{1}{\pi}\int_0^\infty \mathrm{Im}\left[\varphi_I(\omega)\,\mathrm{e}^{-\mathrm{i}\omega x}\right]\frac{\mathrm{d}\omega}{\omega}, \quad x \in \mathbb{R}. \tag{3}$$

2.2. Unslotted ALOHA with central gateway

Let us model the uplink of an interference-limited network system that behaves as unslotted (not slotted) ALOHA with a capture model, *i.e.*, the transmission is successfully received if the SIR is above a given threshold.

This network has n_c class categories, and all user classes transmit to a central node denominated as *gateway*, which can receive only one packet at a time per channel, *i.e.*, there is only one receiver for all user classes considering a given channel.

Supposing that a user from class $i \in \mathcal{N} \triangleq \{1, 2, \ldots, n_c\}$ gains access to the *gateway's* receiver in the server. During the transmission the *gateway* may receive interference from class $j \in \mathcal{N}$. So, denoting this interference as I_{ij} and the threshold for successful communication as θ_{ij}, *i.e.*, if the packet is successfully received, then the ratio $h_i\ell(R_i)/I_{ij} > \theta_{ij}$ holds for all j, where h_i is a rv that represents the fast fading coefficient. Thus, a sufficient condition and more conservative approach for successful packet transmission from ith class is that $h_i\ell(R_i) > \sum_j \theta_{ij} I_{ij}$, and the probability of such event is denoted as coverage probability

$$p_{\mathrm{cov}}^{(i)} \triangleq \mathbb{P}\left(h_i\ell(R_i) > \sum_{j\in\mathcal{N}} \theta_{ij} I_{ij}\right). \tag{4}$$

For a given channel, each user class has incoming traffic, and we assume the time of arrival of packets from class $i \in \mathcal{N}$ follows a Poisson process of parameter λ_i. Also, the period of time a packet uses the channel is denoted by τ_i. A user gains access to the server's *gateway* whenever the channel is free. Thus, this probability is the same for all user classes and it is given by

$$p_{\mathrm{acc}} = \exp\left(-\sum_{i\in\mathcal{N}} p_{\mathrm{acc}}\lambda_i\tau_i\right), \tag{5}$$

since the interarrival times of any Poisson process follow iid exponential distributions. Also, the thinning property from Poisson processes guarantees that the filtered process of users that gained access to the channel is a Poisson process with parameter $p_{\mathrm{acc}}\lambda_i$.

Remark 1. The model can be extended to include more users from different user classes gaining access to the channel at the same time (as it is done in some LoRa systems [13]). However, to simplify the analysis, and find p_{acc} in closed form, we restricted to one user at a time.

The interference from class $j \in \mathcal{N}$ in a typical packet of class $i \in \mathcal{N}$ is given by the rv

$$I_{ij} = \sum_{k=1}^{N_{ij}} Z_{ijk}\ell(R_{jk}), \tag{6}$$

where N_{ij} is the number of interferers and follows a Poisson distribution of parameter $\lambda_j(\tau_i + (1-p_{\mathrm{acc}})\tau_j)$, which consists of the sum of the Poisson process, from the early interferers that did not gain access to the server, of parameter $(1-p_{\mathrm{acc}})\lambda_j\tau_j$ and the Poisson process, from the late interferers, of parameter $\lambda_j\tau_i$; the sequence $\{Z_{ijk}\}_k$ are iid rv that represent the percentage of the typical packet that suffered interference multiplied by the fast fading coefficient for each interferer, and $\{R_{jk}\}_k$ are iid rv that represent the distances of the interferers. Also, when referring to the distributions of the rvs Z_{ijk} and R_{jk}, let us denote as Z_{ij} and R_j, respectively, to lighten the notation, since they are iid on the index k.

2.3. Specifying the final model

From now on, let us suppose the path-loss law $\ell(r) = r^{-\alpha}$, where $\alpha > 0$ is the path-loss exponent [14], the value of α depends on the propagation environment, e.g., for the free space $\alpha = 2$, and for an urban setting with shading $\alpha \in (2, 5)$. Let us neglect fast fading ($h_i = 1, i \in \mathcal{N}$), but let us consider packet superposition, and that each user class $j \in \mathcal{N}$ is distributed homogeneously in a ring with an inner and outer radius of $r_{\mathrm{in}}^{(j)}$ and $r_{\mathrm{out}}^{(j)}$, respectively. Thus, the pdf of R_j and Z_{ij} are given by

$$f_{R_j}(r) = \frac{2\,r}{{r_{\mathrm{out}}^{(j)}}^2 - {r_{\mathrm{in}}^{(j)}}^2}, \quad r \in [r_{\mathrm{in}}^{(j)}, r_{\mathrm{out}}^{(j)}], \tag{7}$$

$$f_{Z_{ij}}(z) = \frac{|\tau_i - \tau_j|\,\delta_{\xi_{ij}}(z) + 2\tau_i}{\tau_i + \tau_j}, \quad z \in [0, \xi_{ij}], \tag{8}$$

where $\xi_{ij} \triangleq \min\{1, \tau_j/\tau_i\}$, τ_j is the size of the interfering packet, τ_i is the size of the typical packet from ith user class and $\delta_\xi(\cdot)$ is the Dirac delta function centered in ξ.

Remark 2. The rv Z has a uniform distribution since the packets' arrival follows a Poisson process in time. It also has the Dirac delta function δ_ξ, which corresponds to the effect of the interfering packet having a different size than the typical packet. For example, if the interfering packet is larger than the typical packet, then $\mathbb{P}(Z = 1) > 0$.

From the distributions (7) and (8), the characteristic functions of the random variables used in the model can be derived analytically using the special function Exponential Integral $E_\beta(z) \triangleq \int_1^\infty \mathrm{e}^{-zt}/t^\beta \,\mathrm{d}t$. The characteristic functions are showed in (9), (10) and (11) which are given in Box I.

Finally, the transmission success probability is given by the following proposition.

Proposition 1. *The transmission success probability for a user of the ith class, $i \in \mathcal{N}$, is given by*

$$p_s^{(i)} = p_{\mathrm{acc}}\, p_{\mathrm{cov}}^{(i)}, \tag{12}$$

where

$$p_{\mathrm{acc}} = \exp\left\{-\mathcal{W}\left(\sum_{i\in\mathcal{N}} \lambda_i\tau_i\right)\right\}, \tag{13}$$

$$p_{\mathrm{cov}}^{(i)} = \frac{1}{2} - \frac{1}{\pi}\int_0^\infty \mathrm{Im}\left[\varphi_{R_i^{-\alpha}}(-\omega)\prod_{j\in\mathcal{N}} \varphi_{I_{ij}}(\theta_{ij}\omega)\right]\frac{\mathrm{d}\omega}{\omega}, \tag{14}$$

$$\varphi_{\frac{1}{R_i^\alpha}}(\omega) = \frac{\delta}{{r_{\text{out}}^{(i)}}^2 - r_{\text{in}}^{(i)2}} \left({r_{\text{out}}^{(i)}}^2 E_{1+\delta}(-\mathrm{i}\omega/{r_{\text{out}}^{(i)}}^\alpha) - r_{\text{in}}^{(i)2} E_{1+\delta}(-\mathrm{i}\omega/r_{\text{in}}^{(i)\alpha}) \right), \tag{9}$$

$$\varphi_{\frac{Z_{ij}}{R_j^\alpha}}(\omega) = \frac{1}{\tau_i + \tau_j} \frac{\delta}{{r_{\text{out}}^{(j)}}^2 - r_{\text{in}}^{(j)2}} \left[|\tau_i - \tau_j| \left({r_{\text{out}}^{(j)}}^2 E_{1+\delta}(-\mathrm{i}\omega\xi_{ij}/{r_{\text{out}}^{(j)}}^\alpha) - r_{\text{in}}^{(j)2} E_{1+\delta}(-\mathrm{i}\omega\xi_{ij}/r_{\text{in}}^{(j)\alpha}) \right) + \right. \tag{10}$$

$$\left. \frac{2\tau_i}{\mathrm{i}\omega} \left({r_{\text{out}}^{(j)}}^{2+\alpha} E_{2+\delta}(-\mathrm{i}\omega\xi_{ij}/{r_{\text{out}}^{(j)}}^\alpha) - r_{\text{in}}^{(j)2+\alpha} E_{2+\delta}(-\mathrm{i}\omega\xi_{ij}/r_{\text{in}}^{(j)\alpha}) - \frac{{r_{\text{out}}^{(j)}}^{2+\alpha} - r_{\text{in}}^{(j)2+\alpha}}{1+\delta} \right) \right],$$

$$\varphi_{I_{ij}}(\omega) = \exp\left\{ -\lambda_j \left(\tau_i + (1 - p_{\text{acc}})\tau_j \right) \left(1 - \varphi_{\frac{Z_{ij}}{R_j^\alpha}}(\omega) \right) \right\}, \qquad i, j \in \mathcal{N},\ \omega \in \mathbb{R}. \tag{11}$$

Box I.

W is the Lambert-W function and the characteristic functions are given in (9), (10) and (11).

Proof. The random variables that describe the distance, the number of interferers, and the superposition of packets are independent. Then the success probability is given in product form by (12).

Eq. (5) can be solved for p_{acc} using the Lambert-W function to find (13).

Using Gil-Pelaez inversion theorem (shown in (3)) and the characteristic functions, the coverage probability (14) is derived as

$$\begin{aligned} p_{\text{cov}}^{(i)} &= \mathbb{P}\left(R_i^{-\alpha} > I_\Sigma \right) \\ &= \int_0^\infty F_{I_\Sigma}(r^{-\alpha})\, f_{R_i}(r)\, \mathrm{d}r \\ &= \frac{1}{2} - \frac{1}{\pi} \int_0^\infty \mathrm{Im}\left[\varphi_{I_\Sigma}(\omega) \int_0^\infty f_{R_i}(r)\, \mathrm{e}^{-\mathrm{i}\omega/r^\alpha}\, \mathrm{d}r \right] \frac{\mathrm{d}\omega}{\omega} \\ &= \frac{1}{2} - \frac{1}{\pi} \int_0^\infty \mathrm{Im}\left[\varphi_{R_i^{-\alpha}}(-\omega)\, \varphi_{I_\Sigma}(\omega) \right] \frac{\mathrm{d}\omega}{\omega}, \end{aligned}$$

where $I_\Sigma \triangleq \sum_j \theta_{ij} I_{ij}$ and thus $\varphi_{I_\Sigma}(\omega) = \prod_j \varphi_{I_{ij}}(\theta_{ij}\omega)$, which ends the proof. □

Remark 3. Notice that what defines $p_{\text{cov}}^{(i)}$ in (4) is directly related to the ratio $\dfrac{\ell(R_i)}{\sum_{j\in\mathcal{N}} \theta_{ij} I_{ij}}$ (when $h_i = 1$), which is the SIR, and for the present scenario can be written as

$$\frac{R_i^{-\alpha}}{\sum_{j\in\mathcal{N}} \sum_{k=1}^{N_{ij}} \theta_{ij} Z_{ijk} R_{jk}^{-\alpha}} = \left(\sum_{j\in\mathcal{N}} \sum_{k=1}^{N_{ij}} \theta_{ij} Z_{ijk} \left(\frac{R_i}{R_{jk}} \right)^\alpha \right)^{-1}. \tag{15}$$

Therefore, the SIR distribution, at hand, depends exclusively on the distributions of $(R_i/R_{j1})^\alpha$, Z_{ij} and N_{ij}, for all $j \in \mathcal{N}$. From this, two important properties are observed in the current model:

(Pr1) The system behavior does not change by a multiplicative factor on the random variable vector of distances $[R_j]_{j\in\mathcal{N}}$;

(Pr2) Increasing the path-loss exponent α, increases the SIR when the transmission distance is smaller than the interferer distance, and decreases the SIR when the transmission distance is bigger than the interferer distance.

The following proposition results when $\alpha \to \infty$ in a communication system is limited by interference. It is helpful to analyze the system's asymptotic behavior as the path loss exponent α is increased, such as we do in Section 4.3.

Proposition 2. *If $\alpha \to \infty$, $r_{\text{in}}^{(j)} = 0$ and $r_{\text{out}}^{(j)} = r_{\max}$ for all $j \in \mathcal{N}$, the success probability of the ith class is given by*

$$p_s^{(i)} = p_{\text{acc}} \frac{1 - \mathrm{e}^{-\upsilon_i}}{\upsilon_i}, \quad i \in \mathcal{N},$$

where $\upsilon_i = \sum_{j\in\mathcal{N}} \lambda_j(\tau_i + (1 - p_{\text{acc}})\tau_j)$.

Proof. First, let us note, in (15), that when $R_i < R_{jk}$, then $(R_i/R_{jk})^\alpha \to 0$. On the other hand, if $R_i > R_{jk}$, then $(R_i/R_{jk})^\alpha \to \infty$. Thus, it is easy to see that we have successful transmission if, and only if, $R_i < R_{jk}$ for all $j \in \mathcal{N}$ and $k \in \{1, \ldots, N_{ij}\}$. Otherwise, we have SIR = 0. The case where $R_i = R_{jk}$ is Lebesgue negligible. By symmetry of the random variables $\{R_{jk}\}_{j,k}$ in the OFI approach, the probability of the SIR being above the threshold is equal to $1/(1 + \sum_{j\in\mathcal{N}} N_{ij})$. Note that $\sum_{j\in\mathcal{N}} N_{ij}$ is also Poisson distributed with parameter υ_i, then we can decondition on $\sum_{j\in\mathcal{N}} N_{ij}$ to find a closed form for

$$p_{\text{cov}}^{(i)} = \sum_{k\geq 0} \frac{1}{k+1} \frac{\upsilon_i^k}{k!} \mathrm{e}^{-\upsilon_i} = \frac{1 - \mathrm{e}^{-\upsilon_i}}{\upsilon_i},$$

which, along with Proposition 1, concludes the proof. □

The simplification of the success probability from Proposition 1 to Proposition 2 is remarkable since, in the former, we have to solve an intricate integral numerically; in the latter, we have a closed-form. Therefore, depending on the system's analysis, Proposition 2 is more valuable since it captures the trends of the system concerning the parameters λ and τ. If λ is small for all user classes, this result is a first-order approximation.

3. LoRa technology

Let us apply this model in the uplink of a Long Range (LoRa) system [3], for which we compare with simulations obtained from the LoRa module in software NS-3.[7] [15] The coverage area was limited in all scenarios so that all SFs could be assigned anywhere in the area, ensuring that there was no packet loss by sensitivity.

For all use cases, the following configurations were used in the LoRa module by NS-3[8] [16]: channel long-distance propagation model with path-loss exponent $\alpha = 3.76$ (for the shadowed urban scenario); geographical positions of nodes are taken as a snapshot and modeled with a uniform distribution on a coverage area defined by a disk $r_{\max} = 1000$ m (we carried out this study considering a small-scenario like an

[7] https://github.com/heldercs/projectLoRaWAN.

[8] Typical characteristics of a LoRaWAN network, having regional parameters for different regulatory regions worldwide.

indoor industrial plant, and thus, all SFs are feasible options to send data from the transmitter nodes to the gateway), thus ensuring that all nodes can assign any SFs without loss of sensitivity; bandwidth $BW = 125$ kHz; eight distinct channels are available (equally spaced between 867.1 MHz and 868.5 MHz) to ensure that the six SFs can be assigned anywhere in the coverage area without loss of sensitivity; 1% duty cycle[9]; and coding rate CR = 1. Note that the number of transmissions (NbTrans) is not considered because retransmission are not considered in this work.

LoRa provides a compromise of sensitivity versus data transmission rate, in which the nominal bit rate ranges from 0.3 kbps to 27 kbps. The packet duration is based on the period of the symbol, T_s. This packet duration is the time it takes to send 2^{SF} chips at chip speed, so remember that bandwidth defines the chip rate; it is given by:

$$T_s = \frac{2^{SF}}{BW},$$

where SF can assume integer values between 7 and 12, and having a variety of available bandwidths, defined by [17], and, without loss of generality. For a given combination of SF, CR, BW, and payload (PL) the total transmission time of a LoRa packet is calculated as follows:

$$\tau = \left(20.25 + \max\left(\left\lceil \frac{(4\cdot PL - SF + 11)}{SF} \right\rceil (CR + 4), 0\right)\right)\cdot T_s$$

where $\lceil\cdot\rceil$ refers to the ceil function, which gives the least integer greater than or equal to its argument. Based on the definitions above, we have that the transmission time of a LoRa packet, also defined as Time on Air (ToA), depends on the SF and the packet size (PL) for fixed values of BW and CR.

The LoRaWAN defines some device classes[10]: A, B, or C [3]. In the present work, we use class A, which supports both downlink and uplink communication. However, only the latter is mandatory. The node can send an uplink message at any time and opens two reception windows (for downlink) at specified times of 1 s and 2 s after the uplink transmission.

In this studied scenario, we have nodes homogeneously distributed over the coverage area defined as a circle of radius r_{max}, one central gateway, and $M = 8$ different logical channels. Each node belongs to one of the available user classes depending on its position in space.[11]

The ith class has an area defined by an annulus with internal radius $r_{in}^{(i)}$ and external radius $r_{out}^{(i)}$ (assuming $r_{in}^{(i)} < r_{out}^{(i)}$). The N annuli partition the total space of a disk of radius r_{max}, or they may show some overlap. A sufficient condition to ensure that each node has an assigned SF is that for all $r \in (0, r_{max}]$, there exists an $i \in \mathcal{N}$ such that $r_{in}^{(i)} \le r \le r_{out}^{(i)}$.

Each user class is allocated to a different SF, a key feature of signals based on chirp spreading spectrum (CSS) modulation, such as LoRa. The SF serves as a throughput-range trade-off and also provides an additional dimension for multiple access protocols [18].

To apply our analytical model, let us use the SIR threshold for successful communication θ_{ij}, given in Table 2, for $i, j \in \mathcal{N}$. The rate of packets per channel for the ith class can be calculated as

$$\lambda_i = \frac{n_i\, a_i}{M}, \tag{16}$$

[9] For sub-bands **g** as regulated by ETSI EN300.220 recommendation.

[10] It is essential to note that *device classes* is different from *user class*.

[11] Note that, in theory, there is the possibility to use forty-eight demodulators at the gateway (from six SFs with eight logical channels each. In practice, though, this is unfeasible because of hardware limitations. In this paper, we consider only eight demodulators for two reasons: (i) to include this actual hardware limitation, and (ii) to improve the visualization of the numerical results. The increase of actual parallel transmissions, although possible, would decrease the individual throughputs following the interference analysis presented before. This, however, is not expected to modify the qualitative relations presented next.

Table 2
Thresholds θ_{ij} of SIR, in dB, for the possible combinations of spreading factors desired and interfering signals [19].

ith desired	jth interfering signal		
signal	SF7	SF8	SF9
SF7	6	−16	−18
SF8	−24	6	−20
SF9	−27	−27	6

Table 3
Characteristics of each user class.

User class	SF	a [1/s]	τ [ms]
1	7	0.1	66.8
2	8	0.1	123.4
3	9	0.1	226.3

in which n_i is the number of nodes in the ith class, a_i is the rate of arrival of packets per node from the ith class, and M is the number of logical channels. A channel is randomly chosen with equal probability for each transmission.

The transmission time τ_i of packets from the ith user class and the corresponding SF utilized are showed in Table 3.

Since the nodes are homogeneously distributed over each ring, we have that

$$n_i \le \frac{r_{out}^{(i)\,2} - r_{in}^{(i)2}}{r_{max}^2}\, n,$$

in which $n = \sum_{i=1}^{n_c} n_i$ is the total number of nodes and $r_{max} = \max_{i\in\mathcal{N}} \left\{ r_{out}^{(i)} \right\}$ is the radius of the coverage area, which can be set to one unit of distance without loss of generality (see Pr1 of Remark 3).

4. Numerical results and discussion

4.1. SF allocation schemes

We studied the SF allocation schemes splitting the nodes into two user classes based on their position. In the classical technique, a circumference centered in the gateway with a radius $r_{max} = 1$ unit of distance defines a disk that contains an inner and an outer ring. Different SFs will be allocated to the nodes inside the different rings. The primary approach is to allocate SF 7 to inner and SF 8 to outer rings, which we call *no intersection*. As a counter-proof, we also defined an inverse approach, where the inner ring takes SF 8, and the outer ring takes SF 7, which we call *inversed no intersection*.

The classical approach considers no intersection between the two rings' coverages, but we also investigate it in the intersection's face, be it full or partial. Since there exist infinite possibilities of partial intersections, we have taken only the one that provided the best results, which we call *optimal intersection*. In the *full intersection* approach, the outer and inner rings become coincident, i.e., there is no actual SF allocation based on space position, only in the percentage of users for each SF.

For $n = n_1 + n_2 = 1000$ nodes, Fig. 1 brings the results of system throughput as a function of the proportion of n_1 nodes for those different intersection possibilities, where n_1 is the number of first-class nodes allocated with SF 7 and n_2 is the number of second-class nodes allocated with SF 8.

Note that maximum throughputs are not found with the highest values of n_1 but over proportions between 70% and 85% of SF 7 usage. The throughput curve's optimum point is determined by the balance of characteristics of ToA, quasi-orthogonality, and sensor position. This balance holds for all available curves. When comparing the curves, it is notable how close the full intersection performance is to the optimal intersection because it is independent of the nodes' spatial position.

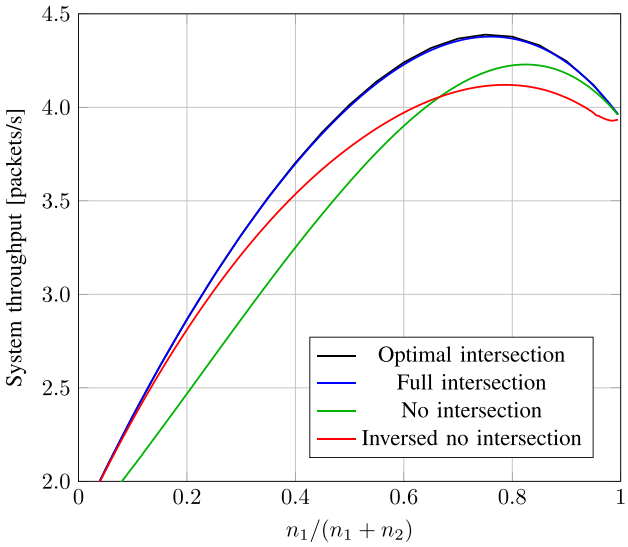

Fig. 1. Intersection schemes comparison: No Intersection, Inversed No Intersection, Full Intersection and the best cases of intersection over n_1/n named Optimal Intersection. For $n = 1000$ nodes and two classes with the first using SF 7 and the second using SF 8.

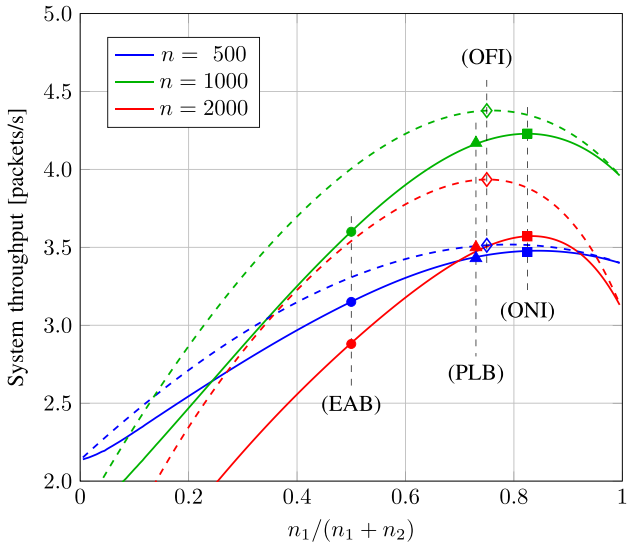

Fig. 2. Performance comparison for No Intersection (solid lines) and Full Intersection (dashed lines) cases. For two user classes with n_1 using SF 7 and n_2 using SF 8.

Fig. 2 shows again system throughput versus first-class proportions but for a slightly different point of view. We gathered just the full intersection (dashed lines) and no intersection (solid lines) results parameterized for some total numbers of nodes (discerned by colors). From that, we have taken some essential vertical marks, such as Equal Area Based (EAB), Path-Loss Based (PLB), Optimal No Intersection (ONI), and Optimal Full Intersection (OFI).

- EAB uses equal-area annuli, where there is *no intersection* between the areas;
- PLB defines annuli based on a path loss model and there is *no intersect*ion between the areas;
- ONI refers to the user-class proportion at which *no intersection* curves reach maximum throughput values;
- OFI refers to the user-class proportion at which *full intersection* curves reach maximum throughput values.

As we have seen previously in Fig. 1, the gain from adopting Optimal Partial Intersection (OPI) approach is negligible compared to the OFI, which has a much simpler implementation. Thus, we have no longer used the OPI strategy.

An important behavior seen in the curves of Fig. 1 and confirmed in Fig. 2 is that a larger transmission time τ results in a significant loss for the network throughput. The worst throughput performance when the $n_1/(n_1 + n_2)$ tends to zero, meaning that the $n_2/(n_1 + n_2)$ tends to one, having the majority of the nodes assigned to SF 8, which has a larger τ. In contrast to the tendency acting in the lower SF's direction due to τ, there is another counter tendency caused by quasi-orthogonality, which requires different user classes; this trade-off defines the maximum throughput of the system. There exists an optimum distribution of the nodes that use SF 7 and SF 8 (n_1 and n_2) that combines the benefits of small τ and quasi-orthogonality.

The position of the sensors acts directly on performance (see Eq. (4)). When we define an area for operation of n_1 or n_2, we hamper the network's performance; that is, we have the best performance for the FI approach, where the position of the sensor is independent of the class. An observation to be noted in Fig. 2 is that the maximum points for the NI and FI approaches are independent of the total number of n nodes, i.e., for $n = 500$, $n = 1000$, or $n = 2000$ the maximum points are aligned with a vertical dashed line. The effects of τ and quasi-orthogonality are related to the n_i/n ratio (not to the total number n of nodes), and the effects of geographical distribution are seen in the difference between continuous (NI) and dashed (FI) curves.

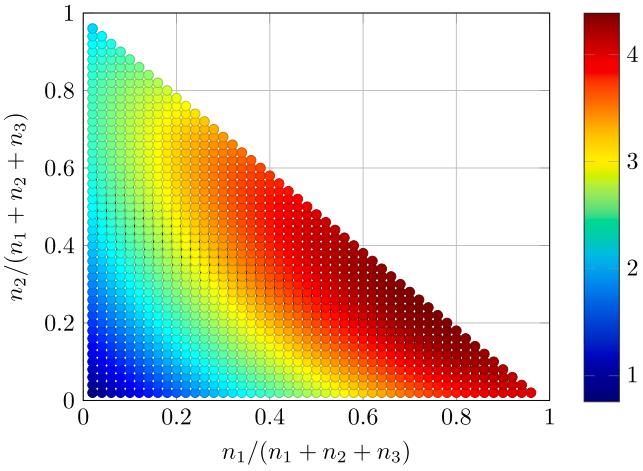

Fig. 3. System throughput for $n = 1000$ nodes split into three user classes and using OFI strategy. First, second and third classes use SF 7, 8, and 9, respectively.

Fig. 3 illustrates the colormap of system throughput values gathered from OFI over $n = 1000$ nodes assigned for three user classes: n_1 refers to nodes with SF 7; n_2 to nodes with SF 8; and, n_3 to nodes with SF 9. We only show the normalized n_1/n and n_2/n axes, since n_3/n is straightly obtained by $n_3/n = 1-n_1/n-n_2/n$. For example, the descendant diagonal edge corresponds to $n_3/n = 0$ and the origin correspond to $n_3/n = 1$ (the worst throughput, as expected). As in previous results, the best throughput is achieved when most nodes are using SF 7. In this way, the long ToA of others will appear only when quasi-orthogonality benefits are the most expressive.

4.2. Mathematical model vs. simulations

In Figs. 4 and 5 we have the mathematical model (solid lines) and simulation (the x marks) results for the EAB, PLB, ONI and OFI approaches with two and three user classes, and total nodes n ranging from 0 to 2000. The probability of success p_s is computed as the weighted average of the packet's probability of success multiplied by the proportion of nodes of each class; the throughput is the sum of all

Table 4
The proportion for each class to four approaches used.

Number of classes	Proportion per class	Approaches EAB	PLB	OFI	ONI
2	n_1/n	50%	73%	82%	76%
	n_2/n	50%	27%	18%	24%
3	n_1/n	$33.\bar{3}\%$	55%	78%	74%
	n_2/n	$33.\bar{3}\%$	22%	18%	24%
	n_3/n	$33.\bar{3}\%$	23%	4%	2%

user classes throughputs. Each marked point was averaged over five independent simulation campaigns, and low deviations were observed. For instance, among all loads and allocation strategies in Fig. 4, the highest standard deviation obtained for system throughput was 0.177 packet/s; in Fig. 5 it was 0.129 packet/s.

Table 4 shows the settings for proportion to n_1 and n_2, as seen in Fig. 4, the OFI and ONI cases are the best ones, where the small difference in favor of OFI is due to the independence of nodes distribution from the class. As the number of nodes in the first class n_1 of PLB is close to ONI and OFI, the results were close to each other. The values of the ONI results for 2 and 3 user classes are coherent with the results in [6]. The worst case is EAB because the first-class n_1 has the same number of nodes of the second-class n_2, providing a higher ToA and, consequently, a greater probability of collision packets.

As seen in Figs. 4, 5 also presents the cases OFI and ONI as the best ones (proportion for n_1, n_2, and n_3 in Table 4), keeping the small difference in favor of OFI due to the nodes' distribution to be independent of the user classes. There was a fall in EAB and PLB metrics, compared to the example of two user classes; it is due to the redistribution of n between n_1, n_2, and n_3, which does not take into account the ToA and quasi-orthogonality characteristics.

The difference between the simulation and the analytical model is that we do not consider the *duty cycle* in the mathematical model because it limits the minimum inter-arrival of packets in a node. Including this effect in the arrival process would make it non-Poissonian and not analytically tractable.

By inspection, it is easy to find the maximum throughput for each strategy since the throughput function is a monotonic increasing function from zero nodes until the global maximum. Then it is a monotonic decreasing function from the global maximum until positive infinity.

4.3. Analysis with path-loss exponent

In this subsection, we explore the effect of the path-loss exponent α in the best performing allocation scheme so far, which is the OFI approach.

Fig. 6 illustrates the effect of α on the throughput and the optimum ratio of the OFI approach. The first plot shows the system throughput as a function of α. The dashed curves are the asymptotes as $\alpha \to \infty$, which are obtained by using Proposition 2 and $n_1/n \to 1$. Due to the system's limitation in terms of interference, the throughput increases with α. For a more significant number of sensors n, there is a greater variation on the throughput concerning α, showing that the path-loss phenomena have more influence on the channel for larger values of n. Through Eq. (15) we can analyze the influence of α on the system. The ratio of distances from a desired and an interfering transmitter, R_i/R_{jk}, is raised to the power of α. By taking these exponential ratios for all j's and k's, together with the respective θ's and Z's, we can compute the SIR. Given Z_{ijk} and θ_{ij}, small ratios $(R_i/R_{jk})^\alpha$ lead to a high SIR, improving the chances to overcome the thresholds of Table 2. From Pr2 of Remark 3, we know that for greater values of α, the probability of successful transmission is improved with respect to interferers that are farther from the gateway than the desired transmitter, and the probability deteriorates when interferers are nearer to the gateway. However, in the OFI scheme, we know that both effects apply for all user classes since they are distributed homogeneously throughout the coverage area.

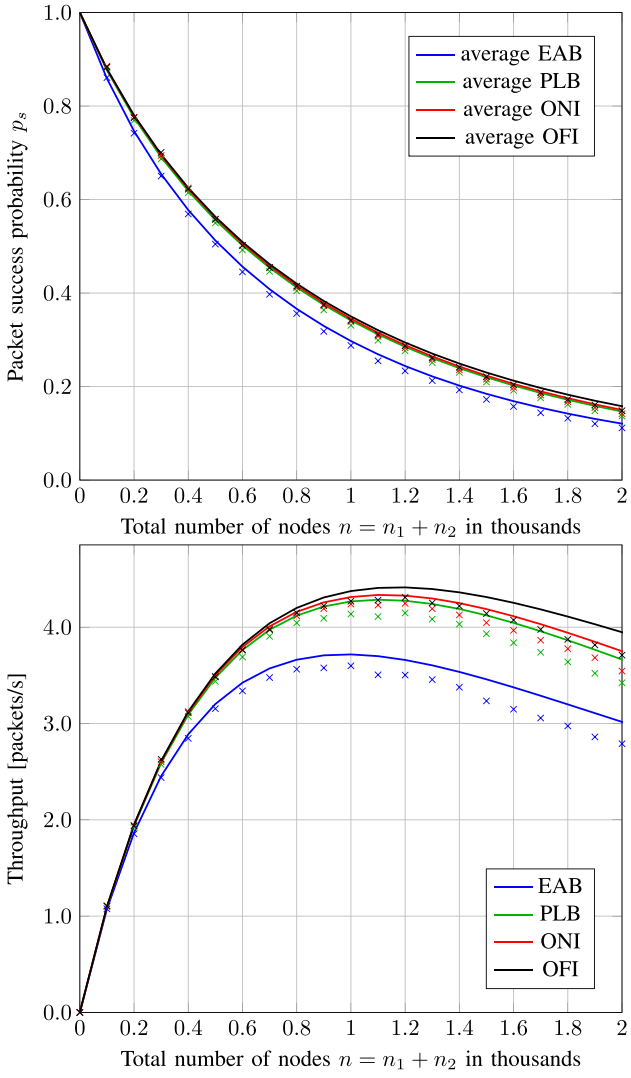

Fig. 4. Packet success probability and system throughput with two user classes (SF 7 and SF 8) for several allocation strategies. The marks correspond to simulation results from NS-3, and the solid lines to the analytical model.

The second plot of Fig. 6 shows the optimal n_1/n proportion as a function of the path-loss exponent α, where each curve can be approximated by an increasing linear function with angular coefficient $a > 0$ representing this increase. We can say that the effect of a decreasing as the number of nodes n increases is caused by the influence of α on the ratio R_i/R_{jk}, meaning that the greater the density of nodes, the greater will be the proportion of interfering signals being further away from the gateway than the desired signal. By varying α from a free space setting ($\alpha = 2$) to a shaded urban setting ($\alpha = 5$), we observe that there is an increase in the proportion n_1/n, showing that increasing the number of nodes with SF = 7 improves performance in a dense urban area, due to the behavior of SIR for an increase in the path loss exponent. The balance of the transmission time and quasi-orthogonal effects lead to a greater n_1/n proportion when α is increased. In resume, the optimal proportion n_1/n grows with α, and its curve slope decreases with the total number of nodes.

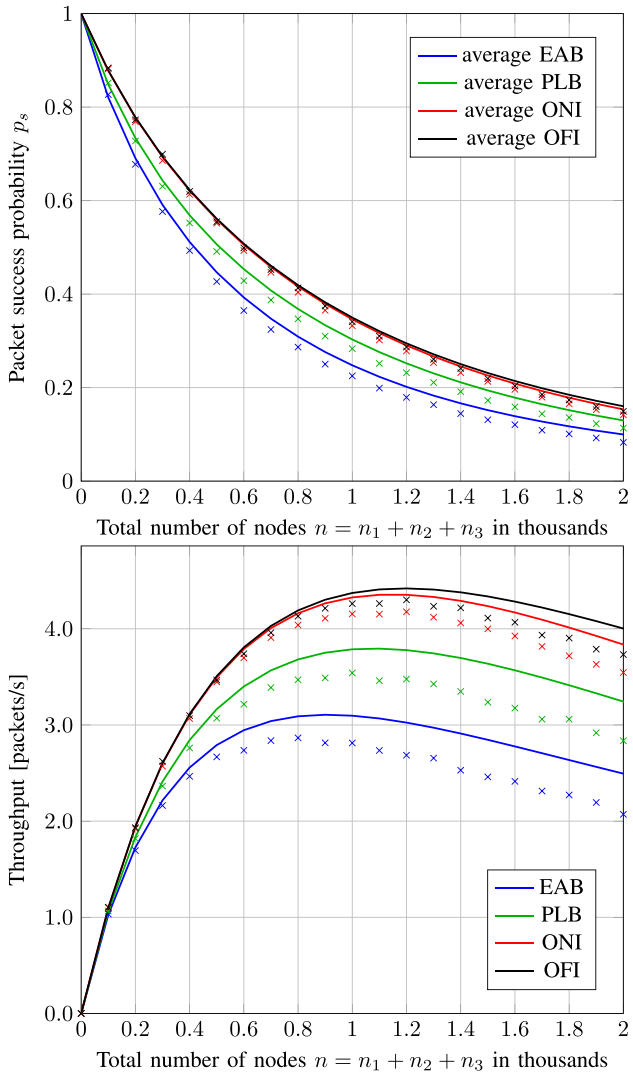

Fig. 5. Packet success probability and system throughput with three user classes (SF 7, SF 8 and SF 9) for several allocation strategies. The marks correspond to simulation results from NS-3, and the solid lines to the analytical model.

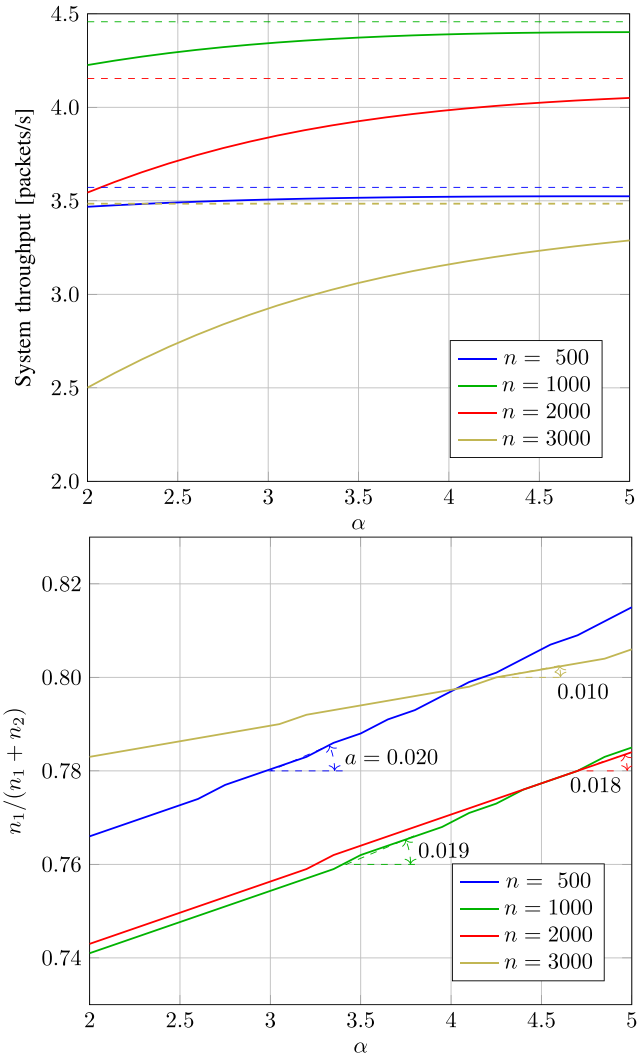

Fig. 6. Two user classes (SF 7 and SF 8) using the OFI strategy. We show the system throughput and the optimal n_1/n as a function of the path-loss exponent α. The dashed curves are the asymptotes as $\alpha \to \infty$.

5. Conclusions and future work

This paper studied an ALOHA-like multi-class random access wireless network based on a newly derived analytical formulation to characterize packet collisions from co-channel interference and thus propose new SF allocation techniques in a LoRaWAN network. We have shown an optimal network throughput, a by-product of the trade-off between success probability and packet collision. Remarkably, we have derived in closed-form the system's asymptotic performance throughput when the path-loss exponent tends to infinity, which can be interpreted as the maximum achievable throughput for such a network.

Moreover, we have numerically compared the results obtained from the proposed analytical formulation with a system-level simulation of LoRaWAN. We have shown that the simulated LoRaWAN system's performance can be reasonably well approximated by our mathematical model, allowing us to compare different SF allocation schemes and the impact of the path-loss on the packet collisions and throughput. We conclude that the use of the spatial allocation technique of SFs is influenced by the action of three effects, which are transmission time τ, the **quasi-orthogonality**, and the ***geographical distribution***. The best allocation strategy is one that balances these three effects, with **OFI** and **OPI** as the best strategies, compared to **EAB** and **PLB** , widely used in the literature.

We expect to extend these results based on our previous contributions to include the possibility of packet retransmissions [20] and other strategies for packet replication [21], as well as by traffic segmentation considering different SF allocation priorities [4]. Besides, we plan to extend the analysis to cover cases, where several LoRa gateways are deployed in a dense region as in [22], utilizing a formulation we have derived for bipolar networks [23].

Declaration of competing interest

The authors declare the following financial interests/personal relationships which may be considered as potential competing interests: Pedro Nardelli, Hirley Alves, Dick Carrillo reports financial support was provided by Academy of Finland. Plinio Dester reports financial support was provided by State of Sao Paulo Research Foundation. Paulo Cardieri reports financial support was provided by Coordination of Higher Education Personnel Improvement.

Data availability

No data was used for the research described in the article.

References

[1] A. Osseiran, J.F. Monserrat, P. Marsch, 5G Mobile and Wireless Communications Technology, Cambridge University Press, 2016.

[2] M. de Castro Tomé, P.H. Nardelli, H. Alves, Long-range low-power wireless networks and sampling strategies in electricity metering, IEEE Trans. Ind. Electron. 66 (2) (2018) 1629–1637.

[3] L. Alliance, LoRaWAN Specifications v1.0.3, LoRa Alliance: Fremont, CA, USA, 2018.

[4] F.H.C.d. Santos Filho, P.S. Dester, E.M.G. Stancanelli, P. Cardieri, P.H.J. Nardelli, D. Carrillo, H. Alves, Performance of LoRaWAN for handling telemetry and alarm messages in industrial applications, Sensors 20 (11) (2020) 3061.

[5] A. Waret, M. Kaneko, A. Guitton, N. El Rachkidy, Lora throughput analysis with imperfect spreading factor orthogonality, IEEE Wirel. Commun. Lett. 8 (2) (2018) 408–411.

[6] D. Zorbas, G.Z. Papadopoulos, P. Maille, N. Montavont, C. Douligeris, Improving LoRa network capacity using multiple spreading factor configurations, in: 2018 25th International Conference on Telecommunications (ICT), IEEE, 2018, pp. 516–520.

[7] O. Georgiou, U. Raza, Low power wide area network analysis: Can LoRa scale? IEEE Wirel. Commun. Lett. 6 (2) (2017) 162–165.

[8] A. Mahmood, E. Sisinni, L. Guntupalli, R. Rondón, S.A. Hassan, M. Gidlund, Scalability analysis of a LoRa network under imperfect orthogonality, IEEE Trans. Ind. Inf. 15 (3) (2018) 1425–1436.

[9] A. Hoeller, R.D. Souza, H. Alves, O.L.A. López, S. Montejo-Sánchez, M.E. Pellenz, Optimum LoRaWAN configuration under Wi-SUN interference, IEEE Access 7 (2019) 170936–170948.

[10] J.-T. Lim, Y. Han, Spreading factor allocation for massive connectivity in LoRa systems, IEEE Commun. Lett. 22 (4) (2018) 800–803.

[11] S. Mohammadi, G. Farahani, Scalability analysis of a LoRa network under inter-SF and Co-SF interference with Poisson point process model, J. Comput. Secur. 8 (2) (2021) 43–57.

[12] J. Gil-Pelaez, Note on the inversion theorem, Biometrika 38 (3–4) (1951) 481–482.

[13] R.B. Sorensen, N. Razmi, J.J. Nielsen, P. Popovski, Analysis of LoRaWAN uplink with multiple demodulating paths and capture effect, in: ICC 2019-2019 IEEE International Conference on Communications (ICC), IEEE, 2019, pp. 1–6.

[14] T.S. Rappaport, Wireless communications–principles and practice, (The Book End), Microw. J. 45 (12) (2002) 128–129.

[15] D. Magrin, M. Capuzzo, A. Zanella, A thorough study of LoRaWAN performance under different parameter settings, IEEE Internet Things J. 7 (1) (2019) 116–127.

[16] L. Alliance, LoRaWAN 1.1 regional parameters, Tech. Specif. (2017).

[17] F. Adelantado, X. Vilajosana, P. Tuset-Peiro, B. Martinez, J. Melia-Segui, T. Watteyne, Understanding the limits of LoRaWAN, IEEE Commun. Mag. 55 (9) (2017) 34–40.

[18] G. Zhu, C. Liao, T. Sakdejayont, I. Lai, Y. Narusue, H. Morikawa, Improving the capacity of a mesh LoRa network by spreading-factor-based network clustering, IEEE Access 7 (2019) 21584–21596.

[19] C. Goursaud, J.-M. Gorce, Dedicated networks for IoT: PHY/MAC state of the art and challenges, EAI Endorsed Trans. Internet Things (2015).

[20] P.H. Nardelli, M. Kaynia, P. Cardieri, M. Latva-aho, Optimal transmission capacity of ad hoc networks with packet retransmissions, IEEE Trans. Wireless Commun. 11 (8) (2012) 2760–2766.

[21] J.M. de Souza Sant'Ana, A. Hoeller, R.D. Souza, S. Montejo-Sánchez, H. Alves, M. de Noronha-Neto, Hybrid coded replication in LORA networks, IEEE Trans. Ind. Inf. 16 (8) (2020) 5577–5585.

[22] H.-C. Lee, K.-H. Ke, Monitoring of large-area IoT sensors using a LoRa wireless mesh network system: Design and evaluation, IEEE Trans. Instrum. Meas. 67 (9) (2018) 2177–2187.

[23] P.S. Dester, P. Cardieri, P.H. Nardelli, J.M. Brito, Performance analysis and optimization of a N-class bipolar network, IEEE Access 7 (2019) 135118–135132.

Francisco Helder C. dos Santos Filho is Adjunct Professor of Federal University of Ceará. He received B.S. degree in electrical engineering from the Federal University of Ceará (UFC - 2001) with a master's degree (2005) and Ph.D. (2021) in Telecommunications Engineering from FEEC - University of Campinas (Unicamp). Worked for 12 years with R&D projects in companies such as Lucent, Nokia Siemens Networks, Datacom, and CPqD, which was the firmware leader for implementing wired and wireless network equipment. Main areas of interest: computer network, IoT radio interfaces, wireless communications, wireless sensor network (WSN), communications protocols, embedded systems, embedded system programming, and Real-Time OS.

Plínio Santini Dester received the B.S. degree in engineering from the École Polytechnique, France, and the B.S. degree in electrical engineering from the University of Campinas, Brazil, following a double degree program, which also conferred the master's degree in 2017. He is currently pursuing the Ph.D. degree in electrical engineering with the University of Campinas (UNICAMP), Brazil. During under graduation, he worked as an Intern with Orange Labs, France, the National Institute for Research in Computer Science and Automation (INRIA), France, the National Center for Research in Energy and Materials (CNPEM), Brazil, and UNICAMP. His research interests include wireless communications and networking, with a focus on theoretical analysis of the performance through stochastic geometry and queueing theory.

Pedro H.J. Nardelli [M'07, SM'19] received the B.S. and M.Sc. degrees in electrical engineering from the State University of Campinas, Brazil, in 2006 and 2008, respectively. In 2013, he received his doctoral degree from University of Oulu, Finland, and State University of Campinas following a dual degree agreement. He is currently Associate Professor (tenure track) in IoT in Energy Systems at LUT University, Finland, and holds a position of Academy of Finland Research Fellow with a project called *Building the Energy Internet as a large-scale IoT-based cyber–physical system that manages the energy inventory of distribution grids as discretized packets via machine-type communications* (EnergyNet). He leads the Cyber-Physical Systems Group at LUT, and is Project Coordinator of the CHIST-ERA European consortium *Framework for the Identification of Rare Events via Machine Learning and IoT Networks* (FIREMAN) and of the project *Swarming Technology for Reliable and Energy-aware Aerial Missions* (STREAM) supported by Jane and Aatos Erkko Foundation. He is also Docentat University of Oulu in the topic of "communications strategies and information processing in energy systems". His research focuses on wireless communications particularly applied in industrial automation and energy systems. He received a best paper award of IEEE PES *Innovative Smart Grid Technologies Latin America* 2019 in the track "Big Data and Internet of Things". He is also IEEE Senior Member. More information: https://sites.google.com/view/nardelli/.

Elvis M.G. Stancanelli received the B.S. degree from the State University of Londrina (UEL), Brazil, in 2002, and the M.Sc. degree from the University of São Paulo (USP), Brazil, in 2004, both in electrical engineering. In 2012 he received the doctoral degree from the Federal University of Ceará (UFC), Brazil, in teleinformatics engineering. From 2004 to 2013, he was with Wireless Telecommunications Research Group (GTEL), Brazil, as a research engineer involved with investigaionts on mobile communications; in autumn 2009, he was a visiting researcher with Ericsson Research, Sweden. Since 2013, he is adjunct professor at UFC. His research interests include wireless and mobile communications, IoT radio interfaces, digital signal processing, computer simulation methods, and machine learning.

Paulo Cardieri received the B.S. degree from the Mauá School of Engineering, Brazil, in 1987, the M.Sc. degree from the University of Campinas (UNICAMP), Campinas, Brazil, in 1994, and the Ph.D. degree from the Virginia Polytechnic Institute and State University, Blacksburg, VA, USA, all in electrical engineering. He is currently an Associate Professor with the School of Electrical and Computer Engineering, UNICAMP. Prior to joining the Faculty of UNICAMP, he was with the CPqD Foundation, Campinas, where he was involved with several research projects on communications, including satellite and wireless communications. From November 1991 to August 1992, he was a Visiting Researcher with the Centro Studi e Laboratori Telecomunicazioni, Turin, Italy. His current research interests include wireless ad hoc networks, sensor networks, and modeling of communication systems.

Dick Carrillo Melgarejo received the B.Eng. degree (Hons.) in electronics and electrical engineering from San Marcos National University, Lima, Perú, and the M.Sc.degree in electrical engineering from Pontifical Catholic University of Rio de Janeiro, Rio deJaneiro, Brazil, in 2004 and 2008, respectively. Between 2008 and 2010, he contributed to WIMAX (IEEE 802.16m) standardization. From 2010 to 2018, he worked with the design and implementation of cognitive radio networks and projects based on 3GPPtechnologies. Since 2018 he is a researcher at Lappeenranta–Lahti University of Technology, where he is also pursuing the Ph.D degree in electrical engineering. His research interests are mobile technologies beyond5G, energy harvesting, intelligent meta-surfaces, Cell-free mMIMO, and RAN Slicing.

Hirley Alves is Assistant Professor and Head of the Machine-type Wireless Communications Group at the 6G Flagship, Centre for Wireless Communications, University of Oulu. He is actively working on massive connectivity and ultra-reliable low latency communications for future wireless networks, 5GB and 6G, full-duplex communications, and physical-layer security. He leads the URLLC activities for the 6G Flagship Program. He has received several awards and has been the organizer, chair, TPC and tutorial lecturer for several renowned international conferences. He is the General Chair of the ISWCS'2019 and the General Co-Chair of the 1st 6G Summit, Levi 2019, and ISWCS 2021.